Journal of Solid State Chemistry 181 (2008) 3294–3302

Contents lists available at ScienceDirect

Journal of Solid State Chemistry

journal homepage: www.elsevier.com/locate/jssc

Substitution features in the isomorphous replacement series for metal-organic compounds $(Nb_xTa_{1-x})_4O_2(OMe)_{14}(ReO_4)_2$, $x = 0.7$, 0.5, 0.3—Single-source precursors of complex oxides with organized porosity

Olesya A. Nikonova, Vadim G. Kessler, Gulaim A. Seisenbaeva *

Department of Chemistry, SLU, Box 7015, 75007 Uppsala, Sweden

ARTICLE INFO

Article history:
Received 14 May 2008
Received in revised form
28 August 2008
Accepted 8 September 2008
Available online 23 September 2008

Keywords:
Rhenium
Niobium
Tantalum
Single-source precursors
Mixed-metal oxoalkoxide
Metal-organic decomposition
Porous oxide

ABSTRACT

Trimetallic oxoalkoxide complexes $(Nb_{0.7}Ta_{0.3})_4O_2(OMe)_{14}(ReO_4)_2$ (**I**), $(Nb_{0.3}Ta_{0.7})_4O_2(OMe)_{14}(ReO_4)_2$ (**II**) and $(Nb_{0.5}Ta_{0.5})_4O_2(OMe)_{14}(ReO_4)_2$ (**III**) were obtained by the interaction of rhenium heptoxide (VII) Re_2O_7 with niobium and tantalum alkoxides $M_2(OMe)_{10}$ (M = Nb, Ta) in toluene. The centrosymmetric molecules (**I**)–(**III**) can be considered as a product of condensation of two $M_2(OMe)_9(OReO_3)$ molecules with the formation of two oxo-bridges. The specific feature of the structure is the uneven distribution of metal atoms in the crystallographic positions, where one symmetry-independent position, connected via μ-O with a perrhenate ReO_4^- group, is predominantly occupied by niobium atoms, while the other one connected via alkoxide groups has a higher tantalum content. The distribution of Nb and Ta in the structure is truly even only for compound **III**. The niobium and tantalum content is varied to a different extent for **I** (less) and for **II** (more), which is apparently due to small differences in the sizes of these two cations, resulting in preferences for packing of different molecules in the structures. Thermal decomposition of $(Nb_{1-x}Ta_x)_4O_2(OMe)_{14}(ReO_4)_2$ ($x = 0.3$, 0.5, 0.7) in air leads to the formation of crystalline species of solid solutions based on tantalum and niobium oxides displaying semi-ordered pores with the size of 100–250 nm. In the dry nitrogen atmosphere, the decomposition leads to the amorphous complex oxides containing rhenium, niobium and tantalum.

1. Introduction

Mixed-metal oxoalkoxide complexes are attractive potential precursors of complex oxide and alloy materials [1]. Rhenium metal has found broad application as a component of catalysts for alkylation in the organic synthesis and for industrial cracking processes [2]. The rhenium(VI) oxide, ReO_3, is used as a heterogeneous catalyst in metathesis reactions [3,4]. The biggest limitation of this catalyst is that ReO_3 can easily be reduced to inactive ReO_2 and all attempts to oxidize it to regenerate ReO_3 result in the loss of volatile Re_2O_7. Hence, it is necessary to create conditions, permitting continuous functioning of these catalysts. Earlier we have shown in our work that incorporating ReO_3 into the NaY zeolite matrix can produce nanocomposites, where this oxide is more stable to the reducing conditions [5,6]. Application of niobium and tantalum oxides as matrices in the in situ synthesis of rhenium oxide-based nanocomposites can offer a cost-efficient approach to materials with enhanced stability to reduction. In the literature, there are recent works on rhenium-based catalysts for the metathesis of olefins CH_3ReO_3/Nb_2O_5 [3,4], which showed high catalytic activity for metathesis of 1-pentene [4]. Mixed oxides of general formula $(Nb_{1-x}Ta_x)_2O_5$ are mainly used as photocatalysts for water decomposition [7,8], catalytic reactions [9], biomaterials [10], nanoporous materials for different applications [10] and materials for optoelectronics [10].

The traditional method of obtaining the multicomponent oxides is usually via standard procedures such as the conventional solid-state reactions between binary oxides. This method was successfully implemented for the preparation of $(Nb_{1-x}Ta_x)_2O_5$ [11], $Bi_3Fe_{0.5}Nb_{1.5}O_9$, [12] and many other refractory materials. Unfortunately, the ceramic method requires heat treatment at rather high temperatures and leads to poorly homogeneous materials consisting of larger particles [13].

There are some alternative methods for obtaining multicomponent Nb or Ta oxides. For instance, mixed oxides $SrNb_2O_6$ and $SrTa_2O_6$ were obtained via thoroughly mixing Nb or Ta hydroxides and commercially purchased strontium hydroxide and prolonged heating at a relatively low temperature ($<400\,^{\circ}C$). The main limitation of this process is that it is multistep and applies

* Corresponding author. Fax: +46 18 673 392.
E-mail address: Gulaim.Seisenbaeva@kemi.slu.se (G.A. Seisenbaeva).

0022-4596/$ - see front matter © 2008 Elsevier Inc. All rights reserved.
doi:10.1016/j.jssc.2008.09.003

the HF acid in the technique applied for the preparation of Nb and Ta hydroxides [14]. Other alternative routes such as sol–gel synthesis based on metal-organic precursors, and the citrate method are often considered. Even the citrate method has such limitations as being a multistep and time-consuming procedure [15]. For instance, $(Nb_{1-x}Ta_x)_2O_5$ solid solutions have been obtained by a neutral templating sol–gel method, using the pentachlorides as metal precursors and a block copolymer as the template. According to this method, it is possible to obtain the mesopours oxide $(NbTa)_2O_5$, which, however, contains chloride impurities [16,17]. The mesoporous mixed oxides based on Nb and Ta or Mo can also be obtained by the thermal decomposition of organic–inorganic precursors with the required ratio of metals in the molecular structure. The syntheses of precursors are complicated and involved several steps, hence providing relatively low yields of the final products [18,19].

Bi- and trimetallic alkoxides complexes can also be used, as precursors of complex oxides that contain required metals at the given ratios. The most generally applied approach in this case is the metal-organic sol–gel synthesis, where nanoparticles of complex oxides (Micelles Templated by Self-Assembly of Ligands, MTSALs [20]) are formed in organic media through the hydrolytic decomposition of precursors. Poor solubility of all the hydroxide components, resulting from hydrolysis in the given media, insures conservation of the stoichiometry. The thermodynamic stability of the target complex oxide phase then enables its formation under milder conditions. The application of a complex precursor in this case facilitates the introduction of proper stoichiometry but is very often not mandatory. Thus, the trimetallic precursors, whose existence was postulated in the alkoxide systems successfully applied for the synthesis of Bi–Sr–Nb perovskite oxide [21] and Ba–Zr–Ti-oxide phases [22,23], were shown in more close studies [24,25] not to be individual compounds, but mixtures of bimetallic species. The application of individual trimetallic precursors appears, in contrast, to be especially attractive in the synthesis of complex oxides via metal-organic chemical vapor deposition and the metal-organic decomposition route, where different thermal stability and volatility of homometallic reactants can be a problem.

Trimetallic complexes based on rhenium, niobium and tantalum of the following formula $(Nb_{0.5}Ta_{0.5})_4O_2(OMe)_{14}(ReO_4)_2$ and $(Nb_{0.5}Ta_{0.5})_2(OMe)_8(ReO_4)_2$ with the Nb:Ta ratio 1:1 have been described earlier in [26]. The synthesis of these complexes was based on the interaction between Re_2O_7 and bimetallic alkoxide of niobium and tantalum, $NbTa(OMe)_{10}$ [27]. It is possible to obtain these compounds due to isomorphous substitution for niobium atoms by tantalum ones, because the ionic radii of Nb^v and Ta^v for coordination number 6 are almost the same and equal to 0.64 Å [28].

The purpose of the present work was to investigate the possibility to obtain new trimetallic oxoalkoxocomplexes on the basis of Re, Nb and Ta in a wider range of compositions and test their applicability for the synthesis of porous complex oxide materials.

2. Experimental

All the preparative procedures were carried out in dry nitrogen atmosphere using a dry box. Toluene was dehydrated by refluxing over $LiAlH_4$ with subsequent distillation. Methanol was purified by distillation over magnesium methoxide.

IR spectra of Nujol and hexachlorobutadiene (HCB) mulls were obtained with a Perkin Elmer FT-IR spectrometer Spectrum-100. Mass-spectra were recorded using a JEOL JMS-SX/SX-102A mass-spectrometer, applying electron beam ionization ($U = 70$ eV) with direct probe introduction. Microanalysis studies of all samples were carried out using a Heraeus CHN-O-RAPID instrument (standard deviations: C ± 0.3%, H ± 0.1%).

Thermal analysis (DTA–TGA) was carried out in air at a heating rate 5 °C/min, using the Q-1500 D instrument (Derivatograph-C, system developed by F. Paulik, J. Paulik, L. Erdey; MOM, Hungary) with 120–300 mg samples (weighing accuracy, ±0.4 mg).

Thermo-gravimetric (TG) studies were carried out with a Perkin-Elmer TGA-7 device and the measurements were performed in nitrogen atmosphere, with the samples of 10–15 mg.

X-ray powder diffraction (XRD) studies were carried out on a DRON-3M powder diffractometer (Cu$K\alpha$ radiation, scan step of 0.05–0.1°, counting time of 2–4 s per data point) and by the Guinier–Hägg method using Cu$K\alpha$ radiation and silicon as the internal standard and with an STADI-P (STOE) diffractometer.

Table 1
Crystal data and details of diffraction experiments for compounds **I**, **II**, and **III**

Samples	$(Nb_{0.7}Ta_{0.3})_4O_2(OMe)_{14}(ReO_4)_2$	$(Nb_{0.5}Ta_{0.5})_4O_2(OMe)_{14}(ReO_4)_2$[a]	$(Nb_{0.3}Ta_{0.7})_4O_2(OMe)_{14}(ReO_4)_2$
Parameters			
Temperature of crystallization (°C)	22	22	22
Crystal system, space group	Monoclinic, $P2_1/c$		
Formula	$C_{14}H_{42}O_{24}Nb_{2.80}Ta_{1.20}Re_2$	$C_{14}H_{42}O_{24}Nb_2Ta_2Re_2$[a]	$C_{14}H_{42}O_{24}Nb_{1.20}Ta_{2.80}Re_2$
M (g/mol)	1444.16	1514.60	1585.03
Parameters of unit cell			
a (Å)	9.845(6)	9.745(9)	10.002(2)
b (Å)	16.001(1)	15.882(1)	13.451(4)
c (Å)	12.331(8)	12.204(1)	14.233(3)
β (deg)	100.860(1)	100.98(2)	109.763(6)
Volume of unit cell V (Å^3)	1908(2)	1854(3)	1802.1(8)
Independent reflection (R_{int})	2179 (0.0706)	5594 (0.0977)	5374 (0.0540)
Observed reflection $I > 2\sigma[I]$	1321	2402	1640
Refined parameters	739	208	200
R_1	0.0868	0.0591	0.0493
wR_2	0.1197	0.1134	0.1001
Goodness of fit	0.974	0.864	0.925

[a] Literature data [26].

The powder patterns were obtained by scanning of the original films using the SCANPI program [29].

For X-ray single-crystal studies, the data collection was carried out at room temperature (r.t.) using a Bruker SMART CCD 1K diffractometer (Mo$K\alpha$ radiation, graphite-monochromator); for the experimental details, see Table 1. The structures were solved by direct methods. Metal atom coordinates were located in the initial solution and all the other non-hydrogen atoms in the subsequent difference Fourier synthesis. All non-hydrogen atoms were refined by full matrix techniques, fist in isotropic and then in anisotropic approximation. The coordinates of the hydrogen atoms were calculated geometrically and introduced in the final refinement in isotropic approximation using a riding model. All calculations were performed using the SHELXTL-NT program package [30] on a personal computer. Empirical adsorption correction was made applying the SADABS program.

SEM micrographs of the samples were obtained in transmission electron microscope HITACHI TM-1000 μDex, equipped with EDS analysis.

The alkoxides, used in this work as starting materials for the synthesis of trimetallic complexes, $Nb_2(OMe)_{10}$ and $Ta_2(OMe)_{10}$, were prepared by anodic oxidation of the corresponding metals in methanol and purified according to conventional techniques [31].

2.1. Synthesis

$(Nb_{0.7}Ta_{0.3})_4O_2(OMe)_{14}(ReO_4)_2$ (I)—Niobium methoxide $Nb_2(OMe)_{10}$ (0.890 g; 1.794 mmol) and tantalum methoxide $Ta_2(OMe)_{10}$ (0.521 g, 0.775 mmol) were dissolved in 3.5 and 2.5 mL of toluene, respectively, and then solutions were poured together and mixed in order to achieve the Nb:Ta = 0.7:0.3 ratio. Rhenium heptoxide (VII) Re_2O_7 (0.618 g; 1.277 mmol) was added to the obtained solution upon stirring and stirred further in 30–60 min at 25–30 °C until Re_2O_7 was dissolved completely. During dissolution of Re_2O_7, the color of solution changed from light green to pinkish-brown. At the end of the process, the mixture was heated to 50 °C and the color of the solution became dark brown with red nuance. Then the mixture was refluxed during 3–5 min and then cooled to r.t. and left for crystallization. After 24 h, the solution was decanted and the crystalline product (thick needle-shaped crystals light lilac in color) was dried in vacuum. Yield: 91%. *Anal.* Calculate for $C_{14}H_{42}O_{24}Nb_{2,80}Ta_{1,20}Re_2$%: C 11.63; H 2.91. Found, %: C 11.67; H 2.95. IR spectrum in Nujol, cm^{-1}: 1109 s br, 995 m br, 930 m br, 890 w br, 805 s br, 721 w, 567 m br, 516 m br. IR spectrum in HCB, cm^{-1}: 1633 w, 1607 m, 1561 s. MS, *m*/*z* (%), interpretation: 641(2.24) $Ta_2(OMe)_9^+$, 595(1.14) $Ta_2O(OMe)_7^+$, 553(3.16) $TaNb(OMe)_9^+$, 507(3.11) $TaNbO(OMe)_7^+$, 461(1.73) $TaNbO_2(OMe)_5^+$, 385(1.35) $TaNbO_2(OH)(OMe)_2^+$, 305(31.21) $Ta(OMe)_4^+$, 266(41.01) $ReO_3(OMe)^+$, 265(40.41) $ReO_3(OCH_2)^+$, 259(5.86) $TaO(OMe)^+$, 251(5.34) ReO_4^+, 249(4.06) $Re(OMe)_2^+$, 248(2.24) $Re(OCH_2)(OMe)^+$ and $Nb(OMe)_5^+$, 247(2.29) $Nb(OMe)_4(OCH_2)^+$, 238(6.38) $Re(OH)_3^+$, 237(6.72) $ReO(OH)_2^+$, 236(71.22) $ReO_2(OH)^+$, 235(35.30) ReO_3^+, 234(40.95) $ReO(OMe)^+$, 233(21.85) $ReO(OCH_2)^+$, 220(17.57) $ReO(OH)^+$, 219(67.76) ReO_2^+, 217(100) $Nb(OMe)_4^+$, 204(7.96) $Re(OH)^+$, 203(35.96) ReO^+ and $Nb(OMe)_3(OH)^+$, 201(22.20) $NbO(OMe)_3^+$, 185(29.33) $Nb(OMe)_2(OCH_2)^+$, 172(7.43) $Nb(OMe)_2(OH)^+$, 171(21.25) $NbO(OMe)_2^+$, 157(5.54) $NbO(OH)(OMe)^+$, 139(9.55) $NbO(OCH_2)^+$, 125(9.95) NbO_2^+.

$(Nb_{0.3}Ta_{0.7})_4O_2(OMe)_{14}(ReO_4)_2$ (II)—Niobium methoxide $Nb_2(OMe)_{10}$ (0.838 g; 1.689 mmol) and tantalum methoxide $Ta_2(OMe)_{10}$ (1.181 g, 1.757 mmol) were dissolved in 3.5 and 2.5 mL of toluene, respectively, and then solutions were poured together and mixed in order to achieve the Nb:Ta = 0.3:0.7 ratio. Rhenium heptoxide (VII) Re_2O_7 (0.618 g; 1.277 mmol) was added to the obtained solution upon stirring and stirred further 30–60 min at 25–30 °C until Re_2O_7 was dissolved completely. Further treatment followed the same procedure as described above for **I**. Yield: 92%. *Anal.* Calculate for $C_{14}H_{42}O_{24}Nb_{1.2}Ta_{2.8}Re_2$%: C 10.60; H 2.65. Found, %: C 10.67; H 2.70. IR spectrum in Nujol, cm^{-1}: 1160 sh, 1106 s br, 995 m br, 941 m br, 927 w, 897 w, 807 m br, 720 w, 566 m br, 533 sh and 496 w br. IR spectrum in HCB, cm^{-1}: 1628 w, 1610 m, 1561 s.

$(Nb_{0.5}Ta_{0.5})_4O_2(OMe)_{14}(ReO_4)_2$ (III)—$(Nb_{0.5}Ta_{0.5})_4O_2(OMe)_{14}(ReO_4)_2$ complex was obtained as described in [4] to compare with complexes (**I**) and (**II**). The niobium and tantalum methoxides $Nb_2(OMe)_{10}$ (1.031 g; 2.079 mmol) and $Ta_2(OMe)_{10}$ (1.394 g; 2.074 mmol) were dissolved, respectively, in 3.5 and 2.5 mL of toluene. Re_2O_7 (0.461 g; 0.952 mmol) was added to the obtained solution upon stirring. Yield: 91%. *Anal.* Calculate for $C_{14}H_{42}O_{24}Nb_2Ta_2Re_2$, %: C 11.09; H 2.77. Found, %: C 10.94; H 2.76. IR spectrum in Nujol, cm^{-1}: 1117 m br, 994 w br, 962 m, 893 w br, 807 m br, 720 w, 564 w br and 512 w br. IR spectrum in HCB, cm^{-1}: 1631 w, 1604 m, 1561 s. MS, *m*/*z* (%), interpretation: 641(2.8) $Ta_2(OMe)_9^+$, 595(4.2) $Ta_2O(OMe)_7^+$, 553(1.7) $TaNb(OMe)_9^+$, 549(1.4) $Ta_2O_2(OMe)_5^+$, 522(0.9) $TaNb(OMe)_8^+$, 517(0.4) $Ta_2(OMe)_5^+$, 508(0.5) $TaNb(OH)(OMe)_7^+$, 507(4.4) $TaNbO(OMe)_7^+$, 503(0.5) $Ta_2(OMe)_4(OH)^+$, 461(2.3) $TaNbO_2(OMe)_5^+$, 446(0.5) $TaNb(OH)(OMe)_5^+$, 429(0.7) $TaNb(OMe)_5^+$, 419(0.9) $Nb_2O(OMe)_7^+$, 415(0.7) $TaNb(OH)(OMe)_4^+$, 399(0.7) $TaNbO_2(OMe)_3^+$, 385(0.6) $TaNbO_2(OH)(OMe)_2^+$, 373(0.6) $Nb_2O_2(OMe)_5^+$, 305(19.0) $Ta(OMe)_4^+$, 281(5.3) $ReO_2(OMe)_2^+$, 275(4.6) $TaO(OH)(OMe)(OCH_2)^+$, 274(1.1) $TaO_2(OMe)(OCH_2)^+$, 267(3.2) $ReO_2(OH)(OMe)^+$, 266(92.1) $ReO_3(OMe)^+$, 265(86.2) $ReO_3(OCH_2)^+$, 259(2.4) $TaO(OMe)^+$, 251(6.0) ReO_4^+, 249(4.6) $Re(OMe)_2^+$, 248(3.0) $Re(OCH_2)(OMe)^+$ and $Nb(OMe)_5^+$, 247(3.0) $Nb(OMe)_4(OCH_2)^+$, 238(9.4) $Re(OH)_3^+$, 237(12.4) $ReO(OH)_2^+$, 236(100) $ReO_2(OH)^+$, 235(51.8) ReO_3^+, 234(96.8) $ReO(OMe)^+$, 233(27.3) $ReO(OCH_2)^+$, 231(2.4) $TaO(OH)_2^+$, 221(3.2) $Re(OH)_2^+$, 220(26.8) $ReO(OH)^+$, 219(95.7) ReO_2^+, 217(72.4) $Nb(OMe)_4^+$, 204(8.0) $Re(OH)^+$, 203(32.3) ReO^+ and $Nb(OMe)_3(OH)^+$, 187(15.3) Re^+, 186(2.3) $Nb(OMe)_3^+$, 172(22.9) $Nb(OMe)_2(OH)^+$, 171(15.1) $NbO(OMe)_2^+$, 157(5.5) $NbO(OH)(OMe)^+$, 155(4.1) $Nb(OMe)_2^+$, 141(3.3) $Nb(OMe)(OH)^+$, 140(2.9) $NbO(OMe)^+$, 139(4.4) $NbO(OCH_2)^+$, 125(5.7) NbO_2^+.

3. Results and discussion

3.1. Characterization of the molecular precursors

3.1.1. Crystal structure

The molecular structure of the obtained complexes $(Nb_{1-x}Ta_x)_4O_2(OR)_{14}(ReO_4)_2$ ($x = 0.3$, 0.5, 0.7) is built up of centrosymmetric molecules (see Fig. 1) that consist of pairs of two MO_6 (M = Nb, Ta) octahedrons. The latter are connected with each other by edges in an equatorial plane and the pairs to each other through a vertex in the axial plane. The $[ReO_4]$ tetrahedrons are attached through a common vertex to one of the two octahedrons in each pair. The perrhenate group is situated in the *trans* position to the bridging oxygen atom (μ-O) connecting the Nb or Ta atoms.

The results of solution and refinement of the structure show significant differences between the unit-cell parameters of the samples (see Table 1). As it can be seen from the results, the unit-cell parameters and standard deviations, i.e., density and volume of unit cell, are depending on the ratio between niobium and tantalum in the complexes.

It was found earlier that the distribution of metals for the $(Nb_{1-x}Ta_x)_4O_2(OMe)_{14}(ReO_4)_2$ complex with $x = 0.5$ in the crystallographic positions in the structure was uneven. The atoms of niobium are mainly placed in the M1 "oxo"-position (see Fig. 1),

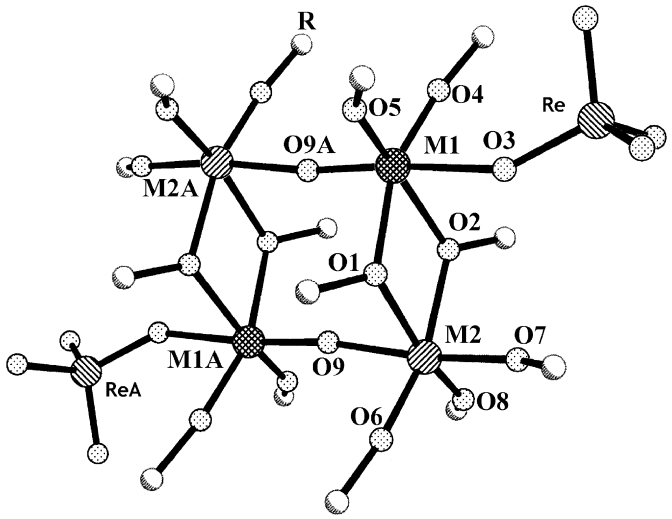

Fig. 1. The molecular structure of $(Nb_{1-x}Ta_x)_4O_2(OMe)_{14}(ReO_4)_2$ ($x = 0.3, 0.5, 0.7$).

Table 2
Metal–oxygen bond lengths in the structure of $(Nb_xTa_{1-x})_4O_2(OMe)_{14}(ReO_4)_2$, $x = 0.3$–0.7

Bond	Sample		
	$(Nb_{0.7}Ta_{0.3})_4O_2(OMe)_{14}(ReO_4)_2$	$(Nb_{0.5}Ta_{0.5})_4O_2(OMe)_{14}(ReO_4)_2$[a]	$(Nb_{0.3}Ta_{0.7})_4O_2(OMe)_{14}(ReO_4)_2$
	Bond length (Å)		
M(1)–O(4)	1.79(2)	1.830(1)	1.865(2)
M(1)–O(5)	1.861(2)	1.855(1)	1.88(2)
M(1)–O(1)	2.078(2)	2.056(1)	2.078(2)
M(1)–O(2)	2.119(2)	2.098(1)	2.119(2)
M(1)–O(9)	1.791(1)	1.791(1)	1.791(1)
M(1)–O(3)	2.214(1)	2.175(9)	2.214(1)
M(2)–O(6)	1.79(2)	1.772(2)	1.79(2)
M(2)–O(8)	1.861(2)	1.878(1)	1.861(2)
M(2)–O(7)	1.887(2)	1.888(1)	1.887(2)
M(2)–O(9)	2.077(1)	2.043(1)	2.077(1)
M(2)–O(2)	2.089(2)	2.066(1)	2.089(2)
M(2)–O(1)	2.086(1)	2.080(1)	2.086(1)
Re(3)–O(3)	1.785(2)	1.727(1)	1.785(2)
Re(3)–O(10)	1.691(1)	1.53(2)	1.691(1)
Re(3)–O(12)	1.690(1)	1.656(2)	1.690(1)
Re(3)–O(11)	1.676(1)	1.67(3)	1.676(1)

[a] Literature data [26].

i.e., the position in which the atom of metal is connected with a perrhenate [ReO_4] group through an oxo-bridge, and the atoms of tantalum are mainly situated in the M2 "alkoxo"-position. Occupation of the first position composes approximately 70% Nb+30% Ta, while the latter one composes 30% Nb+70% Ta [26]. This trend in distribution of metal atoms is preserved for the trimetallic oxoalkoxocomplex with the ratio between Nb and Ta 70:30 according to the structure refinement statistics. For the $(Nb_{0.3}Ta_{0.7})_4O_2(OMe)_{14}(ReO_4)_2$ complex, this distribution is not traced evidently because of the increased tantalum content in the compound. It should thus be concluded that it is the increased niobium content (Nb:Ta = 1:1 and higher) that favours the uneven distribution of metal cations. The contents of niobium and tantalum in the composition of trimetallic complexes influence the parameters and the volume of unit cell, which vary with the increase in the tantalum content and decrease in the niobium content in the oxomethoxocomplexes. The decreasing volume of the unit cell in the series from $(Nb_{0.7}Ta_{0.3})_4O_2(OMe)_{14}(ReO_4)_2$ to $(Nb_{0.3}Ta_{0.7})_4O_2(OMe)_{14}(ReO_4)_2$ is observed from the results of the single-crystal X-ray experiments (see Table 1), and is connected possibly with slightly different polarity of the molecules, resulting in minor differences in the packing density.

The comparison of the M–O bond lengths of the complexes shows that for (**I**) and (**II**) they are similar while for the complex (**III**) a slight shortening of metal–oxygen bonds is observed (see Table 2), which is related to the Nb:Ta ratio in the compounds. This trend is confirmed by analysis of the IR spectra (see Figs. S1, S2) of these complexes.

3.1.2. FTIR spectra

In the spectra recorded in Nujol mulls for all samples (see Fig. S1), the peaks broaden and the intensity of the bands increase in the series from complex (**I**) with Nb:Ta = 70:30 ratio to complex (**II**) where the Nb:Ta ratio is 30:70 (see Table S1). At 1120–1110 cm^{-1} (the spectral region of the stretching and bending vibrations of the C–O and the C–H, respectively) and at 950–930 cm^{-1} (the spectral region of M–O–M stretching vibrations), the increasing intensity of absorption lines from $(Nb_{0.7}Ta_{0.3})_4O_2(OMe)_{14}(ReO_4)_2$ to $(Nb_{0.3}Ta_{0.7})_4O_2(OMe)_{14}(ReO_4)_2$ is observed, which is related to the possibility of niobium to form bonds with higher multiplicity compared with tantalum. For all the samples at 570–550 cm^{-1} and 540–495 cm^{-1} (the spectral region of the M-OR-*term* and of the μ-OR stretching vibrations, respectively) were found the same peaks, which is due to the same geometry and strength of these bonds in the analogous $(Nb_{1-x}Ta_x)_4O_2(OMe)_{14}(ReO_4)_2$ ($x = 0.3$, 0.5, 0.7) structures (see Table 2, Table S1).

Because the Nujol peaks appear in the same region, 1300–1700 cm^{-1}, as the stretching and bending vibrations of C–C, C=C, O–H for the all samples, we recorded spectra in HCB. The peaks corresponding to the CH_3 fragment of the methoxo-groups are clearly seen in these spectra for all samples (see Fig. S2).

3.1.3. X-ray powder study

For identification and characterization of the bulk samples of trimetallic species (**I**) and (**II**), the XRD analysis of powder of the initial complexes was carried out (see Figs. 2 and 3).

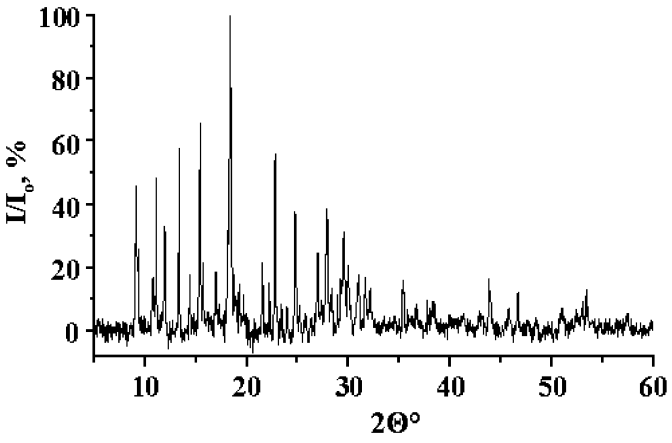

Fig. 2. Powder XRD for $(Nb_{0.7}Ta_{0.3})_4O_2(OMe)_{14}(ReO_4)_2$ (**I**).

The results of identification of the diffractograms and the calculated unit-cell parameters are presented in Table S2, 3. The comparison of the determined unit-cell parameters from powder XRD with the data from single-crystal experiments is presented in Table 3.

The powder patterns (see Figs. 2 and 3) of the initial trimetallic complexes (**I**), (**II**) display rather narrow peaks indicating high crystallinity of the samples. All reflections can be indexed in the unit-cell parameters characteristic of the complexes, which confirms the phase purity of the obtained products.

3.1.4. SEM–EDS study

The SEM analysis of the powders of initial complexes showed that all samples consist of well-shaped crystals (see Fig. 4). The characteristic shapes of the crystals of **I**, **II** and **III** are slightly different: the crystals of **I** were present predominantly as rods, **II**—as blocks and **III**—as thick plates.

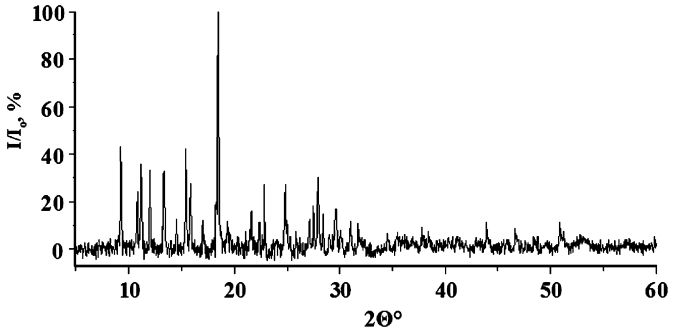

Fig. 3. Powder XRD for $(Nb_{0.3}Ta_{0.7})_4O_2(OMe)_{14}(ReO_4)_2$ (**II**).

Also, the initial complexes were analyzed by the EDS techniques and the statistically sound standard deviations were calculated (see Table 4). The EDS analysis shows (see Table 4) that the crystallization of all complexes from solutions proceeded unevenly, probably because of the partial formation of the individual $(Nb_{0.5}Ta_{0.5})_2(OMe)_8(ReO_4)_2$ as impurity [26]. Some crystals have relatively higher and some—lower Nb:Ta ratio compared with the average values imposed by the conditions of synthesis. The average ratios between Nb, Ta and Re were approximately the same for the samples of (**I**), (**II**) and (**III**) and for the isolated single crystals.

Thus, the results of SEM and powder XRD analyses show that it is possible to synthesize trimetallic complexes on the base of rhenium, niobium and tantalum with a given ratio.

The vapor pressure over the initial complexes (**I**), (**II**) and (**III**) obtained in the present work was studied using tensimetric analysis and has been published separately [32].

3.2. Thermal decomposition

The thermal decomposition of the (**I**), (**II**), (**III**) complexes in air on heating to 1000 °C with the heating rate 5 °C/min studied by TGA revealed two steps of weight loss (see Fig. S3). All samples displayed white–yellowish color and were stable on storage. The first step, apparently, is connected with the thermal decomposition of the complex. The values of weight loss after the first step are close to the theoretical values, calculated for the products presented in Table 5.

The second step, corresponding to the heating above 500 °C (see Fig. S3), is connected with the evolution of rhenium heptoxide (Re_2O_7(g)) into the gas phase. The same type decomposition pathways have earlier been confirmed for bimetallic alkoxides of rhenium and niobium [1], and rhenium and molybdenum [36] using mass-spectrometric identification of the decomposition products. The products of trimetallic

Table 3
The comparison of unit-cell parameters for $M_4O_2(OMe)_{14}(ReO_4)_2$ (M = Nb, Ta) oxomethoxocomplexes from powder XRD and single-crystal data

No.	Complex	a (Å)	b (Å)	c (Å)	β (deg)	V (Å^3)
1[a]	$(Nb_{0.7}Ta_{0.3})_4O_2(OMe)_{14}(ReO_4)_2$	9.812(6)	15.934(9)	12.286(6)	101.24(5)	1883.9(2)
2[a]	$(Nb_{0.3}Ta_{0.7})_4O_2(OMe)_{14}(ReO_4)_2$	9.823(6)	15.974(1)	12.273(6)	101.3(6)	1888.5(2)
3[b]	$(Nb_{0.7}Ta_{0.3})_4O_2(OMe)_{14}(ReO_4)_2$	9.845(6)	16.001(1)	12.331(8)	100.860(1)	1908(2)
4[b]	$(Nb_{0.5}Ta_{0.5})_4O_2(OMe)_{14}(ReO_4)_2$	9.745(9)	15.882(1)	12.204(1)	100.98(2)	1854(3)
5[b]	$(Nb_{0.3}Ta_{0.7})_4O_2(OMe)_{14}(ReO_4)_2$	10.002(2)	13.451(4)	14.233(3)	109.763(6)	1802.1(8)

[a] Powder XRD data.
[b] Single-crystal data.

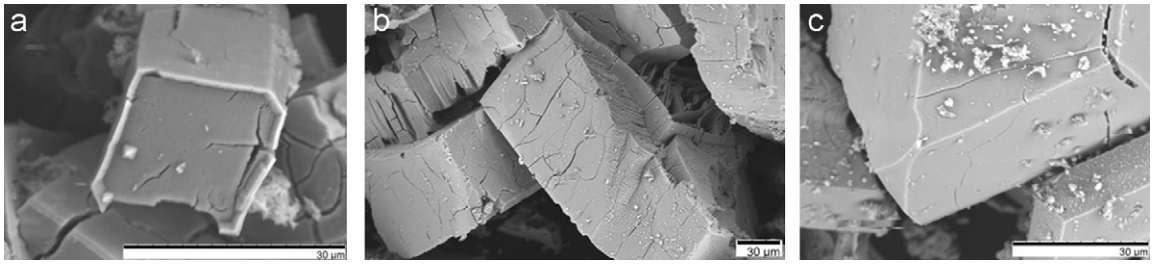

Fig. 4. SEM micrographs of the complexes: a—**I**, b—**II** and c—**III**.

Table 4
The results of EDS analysis for the bulk samples of complexes (**I**), (**II**) and (**III**)

Complex	Metal	Atom (%)	Ratio Nb:Ta	Ratio *M*:Re (*M* = Nb+Ta)
$(Nb_{0.7}Ta_{0.3})_4O_2(OMe)_{14}(ReO_4)_2$	Nb	47.078 ± 0.006	0.720	1.9:1
	Ta	18.316 ± 0.003	0.280	
	Re	34.605 ± 0.001		
$(Nb_{0.5}Ta_{0.5})_4O_2(OMe)_{14}(ReO_4)_2$	Nb	37.733 ± 0.067	0.494	1.8:1
	Ta	32.459 ± 0.014	0.506	
	Re	35.808 ± 0.020		
$(Nb_{0.3}Ta_{0.7})_4O_2(OMe)_{14}(ReO_4)_2$	Nb	21.541 ± 0.046	0.335	1.8:1
	Ta	42.733 ± 0.018	0.665	
	Re	35.726 ± 0.019		

Table 5
The thermal decomposition results in the different atmospheres of trimetallic complexes (**I**), (**II**) and (**III**)

Sample	Condition			Decomposition step			Calculation		Product
	T_{max} (°C)	W_T (°C)	Atmosphere	No.	T (°C)	$-\Delta m$ (%)	$-\Delta m$ (%)	For product	
$(Nb_{0.7}Ta_{0.3})_4O_2(OMe)_{14}(ReO_4)_2$	1000	5	Air	1	80–291	0–21.4	22.3	$(Nb_{0.7}Ta_{0.3})_4Re_2O_{17}$	Phase on the basis
				2	383–450	24.2–25.6	23.4	$(Nb_{0.7}Ta_{0.3})_4Re_2O_{16}$	*L*-modification
				3	515–665		25.7	$(Nb_{0.7}Ta_{0.3})_4Re_2O_{14}$	M_2O_5
						28.6–52.3	55.9	$(Nb_{0.7}Ta_{0.3})_2O_5$	
						56.5			
	950	10	N_2	1	78–416	0–24.5	22.3	$(Nb_{0.7}Ta_{0.3})_4Re_2O_{17}$	Phase on the basis
				2	644–880	26.1–30.5	23.4	$(Nb_{0.7}Ta_{0.3})_4Re_2O_{16}$	*H*-modification
							25.7	**$(Nb_{0.7}Ta_{0.3})_4Re_2O_{14}$**	M_2O_5
					950	31.2	31.6	$(Nb_{0.7}Ta_{0.3})_4ReO_9$	
$(Nb_{0.5}Ta_{0.5})_4O_2(OMe)_{14}(ReO_4)_2$	1000	5	Air	1	80–296	0–22.0	21.3	$Nb_2Ta_2Re_2O_{17}$	Phase on the basis
				2	397–458	22.6–24.7	22.4	$Nb_2Ta_2Re_2O_{16}$	*L*-modification
				3	527–693	25.8–47.9	24.5	$Nb_2Ta_2Re_2O_{14}$	M_2O_5
						52.6	53.2	$Nb_2Ta_2O_5$	
	950	10	N_2	1	83–415	0–23.5	22.4	$Nb_2Ta_2Re_2O_{16}$	Phase on the basis
				2	644–877	25–28	24.5	$Nb_2Ta_2Re_2O_{14}$	*L*-modification
					950	30	30.8	$Nb_2Ta_2Re_2O_8$	M_2O_5
$(Nb_{0.3}Ta_{0.7})_4O_2(OMe)_{14}(ReO_4)_2$	1000	5	Air	1	65–92	0–20.4	20.4	$(Nb_{0.3}Ta_{0.7})_4Re_2O_{17}$	Phase on the basis
				2	383–457	20.9–23.1	21.4	$(Nb_{0.3}Ta_{0.7})_4Re_2O_{16}$	*L*-modification
				3	565–685	25.9–44.2	23.4	**$(Nb_{0.3}Ta_{0.7})_4Re_2O_1$**	M_2O_5
						50.5	50.9	$(Nb_{0.3}Ta_{0.7})_2O_5$	
	950	10	N_2	1	83–417	0–22.1	21.4	$(Nb_{0.3}Ta_{0.7})_4Re_2O_{16}$	Phase on the basis
				2	647–880	23.6–25.5	23.4	$(Nb_{0.3}Ta_{0.7})_4Re_2O_{14}$	*L*-modification
					950	28.2	28.4	**$(Nb_{0.3}Ta_{0.7})_4Re_2O_9$**	M_2O_5

complexes' decomposition are solid solutions of niobium and tantalum oxides with various compositions based on *L*-modification Ta_2O_5.

The mass-spectral investigation of all the three complexes shows that (**I**) and (**III**) are transferred to the gas phase in contrast to (**II**), which is not volatile. For compounds (**I**) and (**III**) the mass-spectra indicated first evaporation of the homometallic Nb and Re species because of the decomposition of complexes and then—of the species with Nb:Ta ratio 1:1.

After the thermal decomposition in air, the products of heat treatment were investigated by using powder XRD analysis. The related powder patterns are presented in Fig. 5. The samples of the decomposition products reveal narrow and very closely situated reflections, indicating high crystallinity (the max temperature of heating in air was 1000 °C) (see Fig. 5). These peaks with high intensity were well resolved and applied for calculation of the unit-cell parameters. Only strong lines, not overlapping with the neighboring peaks, were included in the calculation. Thus, the calculated unit-cell parameters for all samples are presented in Table 6. According to the results of powder XRD analysis for the investigated compositions $(Nb_{1-x}Ta_x)_2O_5$, where $x = 0.3$, 0.5, 0.7, we can consider that isomorphous replacement of Nb with Ta increases the temperature stability domain of the of $L(\gamma)$-modification-related M_2O_5 phase up to 1000 °C. These data confirm the formation of solid solutions of niobium and tantalum oxides $(Nb_{1-x}Ta_x)_2O_5$ on the decomposition of trimetallic complexes $(Nb_{1-x}Ta_x)_4O_2(OMe)_{14}(ReO_4)_2$, where $x = 0–1$.

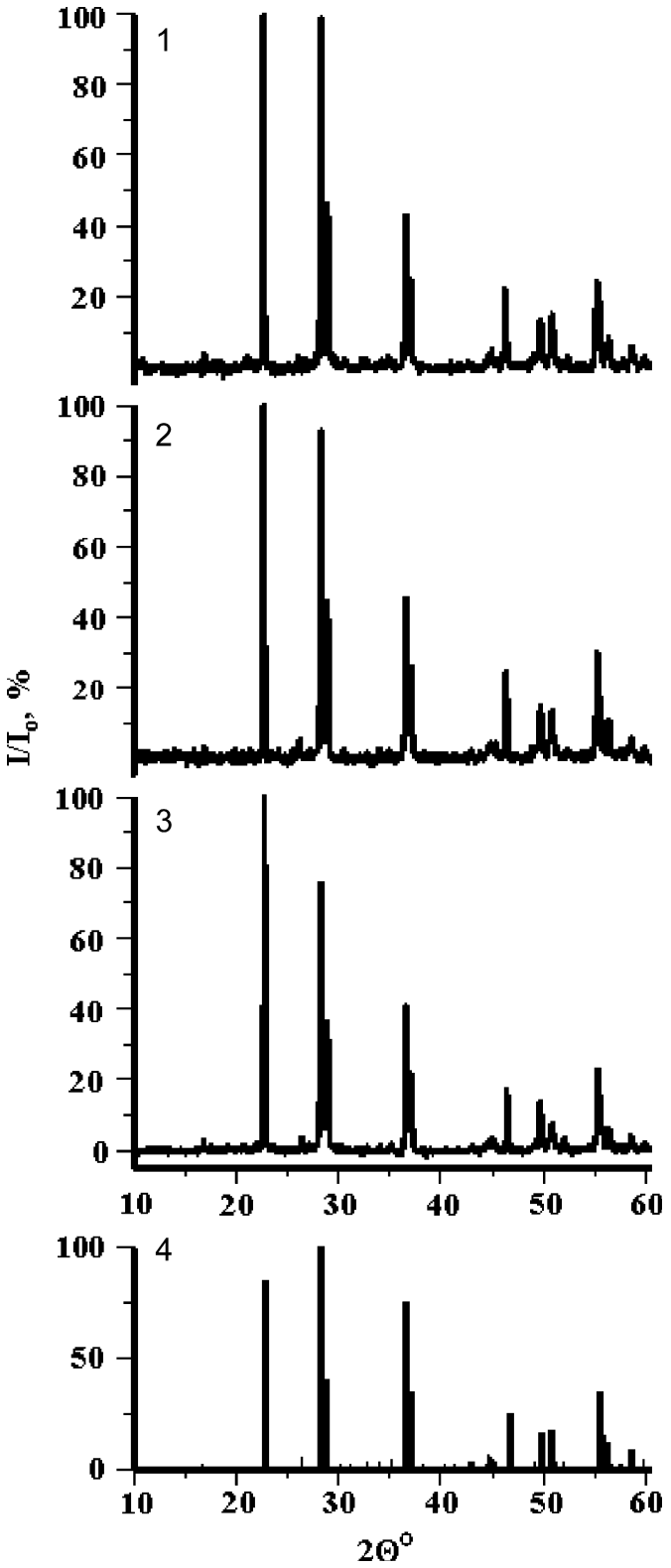

Fig. 5. The X-ray powder patterns of the $M_4O_2(OMe)_{14}(ReO_4)_2$ decomposition products in air (20–1000 °C, 5 °C/min) compared with the literature data: 1—$Nb_{0.7}Ta_{0.3}O_2(OMe)_{14}(ReO_4)_2$; 2—$Nb_{0.5}Ta_{0.5}O_2(OMe)_{14}(ReO_4)_2$, 3—$Nb_{0.3}Ta_{0.7}O_2(OMe)_{14}(ReO_4)_2$ and 4—ICDD-JCPDS data no. 25-0922 for *L*-Ta_2O_5 [33].

The SEM analysis of the products of decomposition shows that all samples contain aggregates, originating from the initial crystals with unchanged size and shape (see Fig. 6) apparently mainly through a solid-state reaction (comp. Fig. 4). The aggregates possess a semi-ordered macroporous structure (see Fig. 6). The size of pores slightly varies and lies in the range of 100–250 nm. The statistically representative EDS analysis has been carried out for the decomposition products (see Table 7). From Table 7, it can be seen that the ratio between Nb and Ta is changed for samples (**I**) and (**II**), which is probably connected with more pronounced partial evaporation of more volatile niobium decomposition intermediates compared with more stable tantalum ones as it was indicated by the mass-spectral investigation. An analogous relation in relative volatility of niobium and tantalum components in a complex has earlier been observed in the classic work of L.G. Hubert-Pfalzgraf on bimetallic niobium–tantalum alkoxides [37].

The thermal decomposition of $(Nb_{1-x}Ta_x)_4O_2(OMe)_{14}(ReO_4)_2$, $x = 0.3, 0.5, 0.7$ was carried out in inert atmosphere on heating to 950 °C at a speed of 10 °C/min. The corresponding TG curves for heating of trimetallic complexes in dry nitrogen atmosphere are presented in Fig. S4. The results of thermal analysis are presented in Table 5.

As can be seen from the thermograms, the process involves two steps, one of which is connected with decomposition of the complex and the second one (⩾500 °C) with the partial loss of rhenium. All products of the decomposition showed metallic luster and appeared to be stable in air. The results of powder XRD have shown that all samples are partially amorphous and represent complex phases presumably containing traces of rhenium. Therefore, all calculations of the cell parameters were made only for lines with essentially high intensity. The powder patterns according to the results of XRD analysis, the decomposition products resulting from the complex $(Nb_{0.7}Ta_{0.3})_4O_2(OMe)_{14}(ReO_4)_2$ contained a phase resembling the monoclinic modification *H*-Nb_2O_5, in contrast to complexes (**II**) and (**III**), which contained phases related to the *L*-modification of Ta_2O_5 (see Table 8). This results most likely from the relatively higher content of tantalum in the two latter materials. Hence, the change in the ratio between niobium and tantalum leads to the formation of different complex oxide phases on the basis of modifications of Nb_2O_5 or Ta_2O_5, respectively (see Table 8). XRD data for all decomposition products are presented in Fig. S5.

We can note that volumes of the unit cells for the Nb:Ta = 50:50 oxide phase and the pure tantalum pentoxide, Ta_2O_5, are practically identical, and the intermediate composition Nb:Ta = 30:70 leads to essentially bigger volumes of the cell. We suggest that intermediate compositions are characterized by more disordered arrangement of cations.

4. Conclusions

Trimetallic complexes of the common formula $(Nb_{1-x}Ta_x)4O_2(OMe)_{14}(ReO4)_2$, with a broad variation of Nb:Ta ratios, can be obtained successfully by the interaction of a mixture of niobium and tantalum alkoxides with rhenium heptoxide. The distribution of Nb and Ta is even at Nb:Ta = 1:1 but is a subject of considerable variation for the Nb- and Ta-rich samples, respectively. The thermal decomposition in air of all the studied complexes $(Nb_{1-x}Ta_x)_4O_2(OMe)_{14}(ReO_4)_2$ ($x = 0.3, 0.5, 0.7$) leads to solid solutions on the basis of *L*-modification of Ta_2O_5 at the temperatures ⩽1000 °C with semi-ordered macroporous structures, where the size of pores lies in the range 100–250 nm. The thermal decomposition in dry nitrogen provides solid solutions on the basis of the *H*-modification of Nb_2O_5 for the niobium-rich precursors and those on the basis of *L*-modification of Ta_2O_5 for Ta:Nb⩾1:1 at the temperature ⩽1000 °C.

Table 6
The comparison of the unit-cell parameters of thermal decomposition products of $M_4O_2(OMe)_{14}(ReO_4)_2$ complexes in air with the literature data

No.	Initial complex	Product	a (Å)	b (Å)	c (Å)	V (Å^3)
1[a]	$(Nb_{0.7}Ta_{0.3})_4O_2(OMe)_{14}(ReO_4)_2$	$(Nb_{0.7}Ta_{0.3})_2O_5$	6.18(6)	40.25(6) = 11 × 3.659	3.922(2)	975.1(2)
2[a]	$(Nb_{0.5}Ta_{0.5})_4O_2(OMe)_{14}(ReO_4)_2$	$(Nb_{0.5}Ta_{0.5})_2O_5$	6.18(6)	40.31(5) = 11 × 3.665	3.918(18)	975.9(2)
3[a]	$(Nb_{0.3}Ta_{0.7})_4O_2(OMe)_{14}(ReO_4)_2$	$(Nb_{0.3}Ta_{0.7})_2O_5$	6.177(1)	40.29(10) = 11 × 3.663	3.909(3)	973(3)
4[b]	$L(\gamma)$-Ta_2O_5 (ICCD-JCPDS no. 25-0922)		6.198(5)	40.29(3) = 11 × 3.663	3.888(5)	970.9
5[b]	$L(\gamma,T)$-Nb_2O_5 (ICCD-JCPDS no. 27-1313)		6.168(1)	29.312(1) = 8 × 3.664	3.938(1)	712.0

[a] Experimental data.
[b] Literature data [33,34].

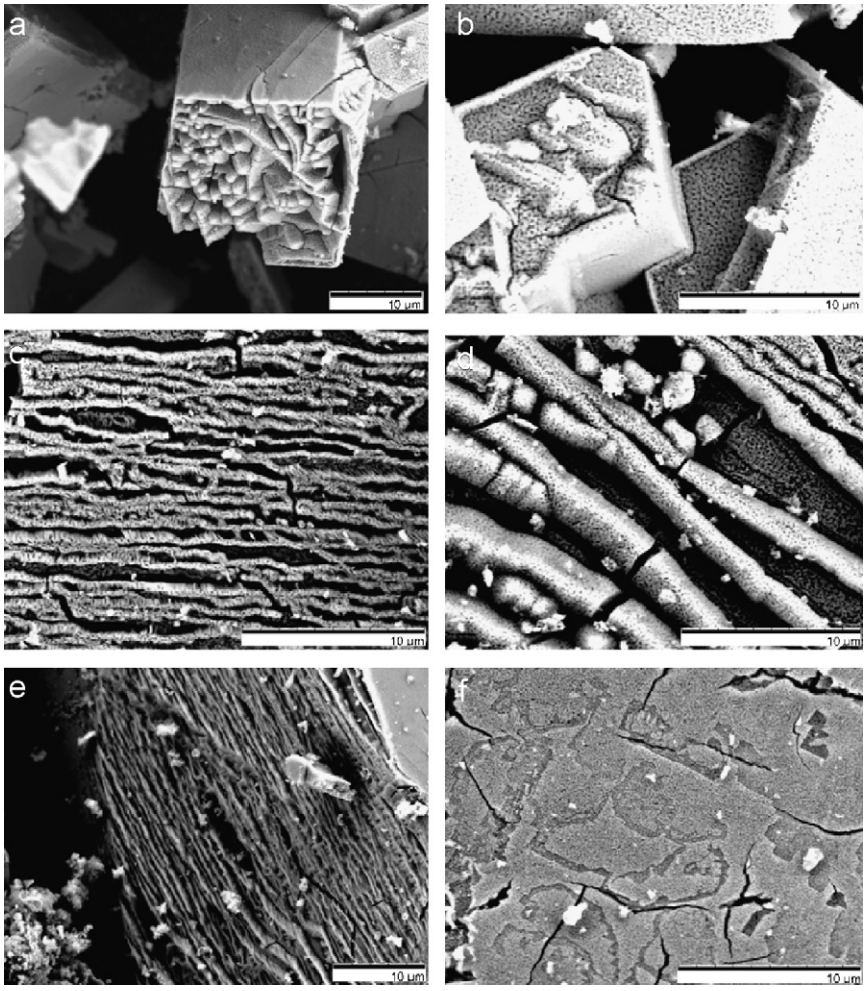

Fig. 6. The SEM micrograph products of decomposition in air: (a,b) $(Nb_{0.7}Ta_{0.3})_4O_2(OMe)_{14}(ReO_4)_2$, (c,d) $(Nb_{0.5}Ta_{0.5})_4O_2(OMe)_{14}(ReO_4)_2$ and (e,f) $(Nb_{0.3}Ta_{0.7})_4O_2(OMe)_{14}(ReO_4)_2$.

Table 7
The results of EDS analysis for the products of decomposition in air

Initial complex	Metal	Atom (%)	Ratio Nb:Ta	Product
$(Nb_{0.7}Ta_{0.3})_4O_2(OMe)_{14}(ReO_4)_2$	Nb	60.474 ± 0.056	0.605	$(Nb_{0.60}Ta_{0.39})_4O_{10+x}$
	Ta	39.526 ± 0.056	0.395	
$(Nb_{0.5}Ta_{0.5})_4O_2(OMe)_{14}(ReO_4)_2$	Nb	49.069 ± 0.002	0.491	$(Nb_{0.49}Ta_{0.51})_4O_{10+x}$
	Ta	50.931 ± 0.002	0.509	
$(Nb_{0.3}Ta_{0.7})_4O_2(OMe)_{14}(ReO_4)_2$	Nb	23.695 ± 0.014	0.237	$(Nb_{0.24}Ta_{0.76})_4O_{10+x}$
	Ta	76.305 ± 0.014	0.763	

Table 8
Comparison of the unit-cell parameters for the products of thermal decomposition of $M_4O_2(OMe)_{14}(ReO_4)_2$ in the dry nitrogen with literature data

No.	Initial complex	Product	a (Å)	b (Å)	c (Å)	V (Å^3)
1[a]	$(Nb_{0.7}Ta_{0.3})_4O_2(OMe)_{14}(ReO_4)_2$	$(Nb_{0.7}Ta_{0.3})_2O_5$	7.24(10)	15.656(10)	7.20(10)	712(16)
2[b]	Nb_2O_5 (ICCD-JCPDS No 27-1312)		7.23	15.7	7.18	712.27
3[a]	$(Nb_{0.5}Ta_{0.5})_4O_2(OMe)_{14}(ReO_4)_2$	$(Nb_{0.5}Ta_{0.5})_2O_5$	6.267(4)	39.84(4) = 11 × 3.622	3.8997(7)	974(12)
4[a]	$(Nb_{0.3}Ta_{0.7})_4O_2(OMe)_{14}(ReO_4)_2$	$(Nb_{0.3}Ta_{0.7})_2O_5$	6.7(10)	39.0(18) = 11 × 3.547	3.891(3)	1020
5[b]	$L(\gamma)$-Ta_2O_5 (ICCD-JCPDS no. 25–0922)		6.198(5)	40.29(3) = 11 × 3.663	3.888(5)	970.9

[a] Experimental data.
[b] Literature data [33,35].

Acknowledgments

The authors express their sincerest gratitude to the Swedish Research council for the financial support and to Mr. Suresh Gohil for the aid in mass-spectrometric experiments. Prof. M. Sundberg is gratefully acknowledged for providing access to TG and X-ray powder techniques and Prof. D.V. Drobot for the help with the elementary microanalysis of the precursor complexes.

Appendix A. Supplementary materials

Supplementary data associated with this article can be found in the online version at doi:10.1016/j.jssc.2008.09.003.

References

[1] P.A. Shcheglov, D.V. Drobot, G.A. Seisenbaeva, S. Gohil, V.G. Kessler, Chem. Mater. 14 (2002) 2378.
[2] J. Xiao, R.J. Puddephatt, Coordin. Chem. Rev. 143 (1995) 457.
[3] R. Buffon, A. Auroux, F. Lefebvre, M. Leconte, A. Choplin, J.-M. Basset, J. Mol. Catal. 76 (1992) 287.
[4] R. Buffon, A. Choplin, M. Leconte, J.-M. Basset, J. Mol. Catal. 72 (1992) L7.
[5] A.L. Kustov, V.G. Kessler, B.V. Romanovsky, G.A. Seisenbaeva, D.V. Drobot, P.A. Shcheglov, J. Mol. Catal. A 216 (2004) 101.
[6] A.L. Kustov, V.G. Kessler, B.V. Romanovsky, G.A. Seisenbaeva, D.V. Drobot, P.A. Shcheglov, Russ. J. Phys. Chem. 78 (2004) S63.
[7] J.N. Kondo, T. Yamashita, T. Katou, B. Lee, D. Lu, M. Hara, K. Domen, Stud. Surf. Sci. Catal. 141 (2002) 265.
[8] Z.G. Zou, H. Arakawa, J.H. Ye, J. Mater. Res. 17 (2002) 1446.
[9] Y. Yue, Z. Gao, Chem. Commun. (2000) 1755.
[10] P. Yang, T. Deng, D. Zhao, P. Feng, D. Pine, B. Chmelka, G. Whitesides, G. Stucky, Science 282 (1998) 2244.
[11] G.P. Mohanty, L.J. Fiegel, J.H. Healy, J. Phys. Chem. 68 (1964) 208.
[12] M.W. Lufaso, W.A. Schulze, S.T. Misture, T.A. Vanderah, J. Solid State Chem. 180 (2007) 2655.
[13] E.R. Camargo, M. Kakihana, Solid State Ion 151 (2002) 413;
H. Wullens, D. Leroy, M. Devillers, Int. J. Inorg. Mater. 3 (2001) 309.
[14] H. Muthurajan, H.H. Kumar, N. Koteswara Rao, Sivaram Pradhan, R.K. Jha, V. Ravi, Mater. Lett. 62 (2008) 892.
[15] I. Truijen, I. Haeldermans, M.K. Van Bael, H. Van den Rul, J.D. Haen, J. Mullens, H. Terryn, V. Goossens, J. Eur. Ceram. Soc. 27 (2007) 4537.
[16] B. Lee, T. Yamashita, D. Lu, J. Kondo, K. Domen, Chem. Mater. 14 (2002) 867.
[17] T. Katou, D. Lu, J.N. Kondo, K. Domen, J. Mater. Chem. 12 (2002) 1480.
[18] N. Deligne, D. Bayot, M. Degand, M. Devillers, J. Solid State Chem. 180 (2007) 2026.
[19] D. Bayot, M. Degand, M. Devillers, J. Solid State Chem. 178 (2005) 2635.
[20] V.G. Kessler, G.I. Spijksma, G.A. Seisenbaeva, S. Håkansson, D.H.A. Blank, H.J.M. Bouwmeester, J. Sol–Gel Sci. Technol. 40 (2006) 163.
[21] K.A. Vorotilov, M.I. Yanovskaya, E.P. Turevskaya, A.S. Sigov, J. Sol–Gel Sci. Technol. 16 (1999) 109.
[22] M. Veith, S. Mathur, N. Lecerf, V. Huch, T. Decker, H.P. Beck, W. Eiser, R. Haberkorn, J. Sol–Gel Sci. Technol. 17 (2000) 145.
[23] N. Lecerf, S. MAthur, H. Shen, M. Veith, S. Hufner, Scripta Mater. 44 (2001) 2157.
[24] S. Parola, These de Doctorat Europeen, University of Nice-Sophia Antipolis, 1996.
[25] G.I. Spijksma, L. Kloo, H.J.M. Bouwmeester, D.H.A. Blank, V.G. Kessler, Inorg. Chim. Acta 360 (2007) 2045.
[26] P.A. Shcheglov, G.A. Seisenbaeva, S. Gohil, D.V. Drobot, V.G. Kessler, Polyhedron 21 (2002) 2317.
[27] L.G. Hubert-Pfalzgraf, J.G. Riess, Inorg. Chem. 14 (1975) 2854.
[28] R.D. Shannon, Acta Crystallogr. A 32 (1976) 751.
[29] G. Malmros, P.E. Werner, Acta Chem. Scand. 27 (1973) 493;
K.E. Johansson, T. Palm, P.E. Werner, J. Phys. E: Sci. Instrum. 13 (1980) 1289.
[30] SHELXTL-NT Reference Manual, Bruker AXS, Madison, WI, 1998.
[31] E.P. Turevskaya, N.Ya. Turova, A.V. Korolev, A.I. Yanovsky, Yu.T. Struchkov, Polyhedron 14 (1995) 1531.
[32] S.N. Mikhnevich, P.A. Shcheglov, D.V. Drobot, Inorg. Mater. 43 (2007) 456.
[33] R.S. Roth, J.L. Waring, H.S. Parker, J. Solid State Chem. 2 (1970) 445.
[34] J.L. Waring, R.S. Roth, H.S. Parker, J. Res. Natl. Bur. Stand. Sect. A 77 (1973) 705.
[35] S. Tamura, J. Mater. Sci. 7 (1972) 298.
[36] G.A. Seisenbaeva, M. Sundberg, M. Nygren, L. Dubrovinsky, V.G. Kessler, Mater. Chem. Phys. 87 (2004) 142.
[37] L.G. Hubert-Pfalzgraf, A.A. Pinkerton, J.G. Riess, Inorg. Chem. 17 (1978) 663.